Magnetic domains in Ni–Mn–Ga martensitic thin films

2005 J. Phys.: Condens. Matter 17 5215

(http://iopscience.iop.org/0953-8984/17/34/006)

INSTITUTE OF PHYSICS PUBLISHING JOURNAL OF PHYSICS: CONDENSED MATTER

J. Phys.: Condens. Matter **17** (2005) 5215–5224 doi:10.1088/0953-8984/17/34/006

Magnetic domains in Ni–Mn–Ga martensitic thin films

V A Chernenko[1,4], R Lopez Anton[2], M Kohl[1], M Ohtsuka[3], I Orue[2] and J M Barandiaran[2]

[1] IMT, Forschungszentrum Karlsruhe, D-76021, Karlsruhe, Germany
[2] Universidad del País Vasco, Departamento de Electricidad y Electrónica, PO Box 644, E-48080 Bilbao, Spain
[3] IMRAM, Tohoku University, Sendai 980-8577, Japan

E-mail: volodymyr_chern@yahoo.com

Received 15 April 2005, in final form 30 June 2005
Published 12 August 2005
Online at stacks.iop.org/JPhysCM/17/5215

Abstract

A series of martensitic $Ni_{52}Mn_{24}Ga_{24}$ thin films deposited on alumina ceramic substrates has been prepared by using RF (radio-frequency) magnetron sputtering. The film thickness, d, varies from 0.1 to 5.0 μm. Magnetic domain patterns have been imaged by the MFM (magnetic force microscopy) technique. A maze domain structure is found for all studied films. MFM shows a large out-of-plane magnetization component and a rather uniform domain width for each film thickness. The domain width, δ, depends on the film thickness as $\delta \sim \sqrt{d}$ in the whole studied range of film thickness. This dependence is the expected one for magnetic anisotropy and magnetostatic contributions in a perpendicular magnetic domain configuration. The proportionality coefficient is also consistent with the values of saturation magnetization and magnetic anisotropy determined in the samples.

(Some figures in this article are in colour only in the electronic version)

1. Introduction

Ferromagnetic thermoelastic martensites formed as a result of the martensitic transformation in Heusler Ni–Mn–Ga shape memory alloys represent new multifunctional materials capable of being activated in a controllable way by temperature, stress, magnetic field or their combination. The engineering of these materials is especially promising for sensing and microactuation, where thin film technology is of prime importance. Thus, a continuing interest exists in the elaboration, characterization and application of these materials in a thin film form. Sputtering technology is commonly used for the preparation of both thick Ni–Mn–Ga films (more than 1.0 μm of thickness) removable from the substrate [1, 2] or being attached to

[4] Author to whom any correspondence should be addressed. On leave from: Institute of Magnetism, Vernadsky street 36-b, Kyiv 03142, Ukraine.

it [3–5] and submicron films which are hardly removable from the substrate due to the natural brittleness of intermetallic compounds [6–8]. Recently, free-standing Ni–Mn–Ga films have been implemented in microdevices, such as a microscanner [9] and a microvalve [10].

The investigation of submicron martensitic Ni–Mn–Ga films is at the beginning. Not only technological but also scientific aspects of such films are interesting to explore. The results reported in the literature are contradictory, since a variety of factors during film preparation come into play, among them the sputtering technique and deposition parameters, the target composition and the substrate nature are worth noting. The martensitic phase in Ni–Mn–Ga alloys is twinned and each twin variant has a large magnetic anisotropy [11, 12]. The transformation behaviour and related properties as well as magnetic characteristics of thin films are largely controlled by crystallography, microstructure and constraint from the substrate, the resulting micromagnetic structure in fine grained films being hardly predictable.

It is worth noting that the correlation between the micromagnetic and twin structure has been already clarified to a large extent in the bulk single-crystalline Ni–Mn–Ga martensitic alloys [13–16] while this issue has been scarcely addressed in martensitic thin films.

The main focus of the present work is a study of the magnetic domain structure, particularly as a function of film thickness for submicron thin films of martensitic Ni–Mn–Ga alloys deposited on alumina substrates.

2. Experimental procedure

Four Ni–Mn–Ga thin films with a thickness of 0.1, 0.4, 1.0 and 5.0 μm were deposited with a radio-frequency (RF) magnetron sputtering apparatus (Shibaura, CFS-4ES) using a target with the nominal composition of $Ni_{52}Mn_{24}Ga_{24}$ (at.%). The film thickness was regulated by the sputtering time. The base pressure in the sputtering chamber was below 2.5×10^{-4} Pa. The sputtering power was 200 W. The atmosphere used for the discharge was high purity argon (>99.9995% Ar) at a flow rate of 230 $mm^3\ s^{-1}$. Alumina ceramic plates, Al_2O_3 (0.15 mm thick, 99.9% of purity, 3.97 g cm^{-3} of density and 0.03 μm of surface roughness) were used as substrates. The substrate temperature was kept at 323 K by cooling water. For homogenization and ordering, the films were heat-treated in vacuum of 2×10^{-4} Pa for 36 ks at 1073 K and then slowly cooled down in a furnace. The composition of the annealed films was determined by the inductive coupled plasma (ICP) method (Seiko, SPS-1200A) to be $Ni_{53.5}Mn_{23.8}Ga_{22.7}$. This composition and heat treatment were tuned to obtain orthorhombic 14 M martensite at room temperature.

The structural characterization was carried out at room temperature by an x-ray diffractometer (Rigaku RINT2200, Cu Kα radiation) in the angle range of $20° < 2\theta < 90°$ with a step of 0.04° and a holding time of 2 s for each step. Transmission electron microscopy (JEOL JEM-2010) was used to confirm the martensitic structure of free-standing 5 μm films peeled off the substrate. The microstructures of chemically etched film surfaces and fractured cross-sections were observed by a scanning electron microscope (SEM JSM 6600).

The transformation behaviour was characterized by the temperature dependences of electrical resistivity which were determined in a vacuum chamber by the four-probe method.

In-plane and out-of-plane magnetization loops at room temperature and the temperature dependences of magnetization at 20 kOe were studied by a SQUID magnetometer (Quantum Design MPMS). The magnetic field-induced signal from the substrate was recorded separately in order to correct the data.

The magnetic force microscopy, MFM, and atomic force microscopy, AFM, measurements were performed with a commercial scanning probe microscope (Nanotec DSP classic) equipped with an in-house built permanent magnet fixture. A NdFeB permanent magnet allows us to

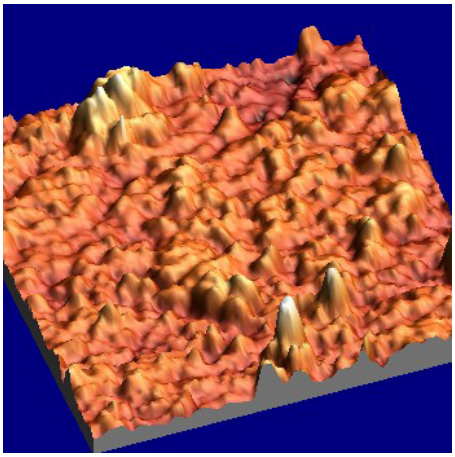

Figure 1. Typical topographic 3D image of the annealed $Ni_{53.5}Mn_{23.8}Ga_{22.7}$ film deposited on alumina substrate. The film thickness is 0.1 μm. The x–y square size is 5×5 μm^2. The vertical axis span is 100 nm.

apply an *in situ* perpendicular-to-plane field of 3.5 kOe at the specimen position. Topographic (height contrast) and magnetic (phase contrast) images were obtained in tapping and tapping-lift mode using standard non-magnetic and magnetic tips. Magnetized CoCr coated etched silicon probe magnetic tips (μMasch NSC18/CoCr, cantilever length 230 μm, resonant frequency $\sim$75 kHz) were used. The typical lift scan height was in the range 50–100 nm. The scan rate varied from 0.5 Hz for large scans ($\sim$30 μm) up to 1 Hz for smaller scans ($\sim$5 μm).

3. Structural and magnetic characterization

Microstructural observations of thin films show in plane a ripple-like surface, which demonstrates an equilibrium-like regular polygonal grain structure after chemical etching with the distribution of the crystallite sizes in the range of 0.1–2.0 μm. For annealed films, this feature is more pronounced. No evidence of the possible presence of a second phase is found. A typical non-etched surface relief is shown in figure 1. The estimated root mean square, rms, roughness and the maximum peak-to-valley range are in the order of 40 and 200 nm, respectively. Note that the former value is correlated with the surface roughness of alumina substrate.

As-deposited submicron films demonstrate in XRD patterns only one weak diffuse peak, which is typical for highly disordered structural states. Annealed films show at least two peaks, see figure 2, after discrimination from the diffraction maxima of alumina. In the latter case, peaks are found only in the interval $40^\circ < 2\theta < 50^\circ$. There is a well pronounced peak, albeit with small intensity, at $2\theta = 48.15^\circ$ but it is not visible in figure 2 due to the scale used. The fragments of x-ray profiles for the alumina and calculated XRD pattern for 14 M martensitic structure are also shown in figure 2 as references. In the calculation, the values of lattice parameters $a = 0.426$ nm, $b = 0.543$ nm, $c = 2.954$ nm, $\alpha = \gamma = 90^\circ$, $\beta = 94.3^\circ$ for 14 M were used [17]. The diffraction patterns of studied martensitic films may be interpreted in terms of 14 M structure with the lattice parameters being approximately equal to $a \approx 0.423$ nm, $b \approx 0.539$ nm and $c \approx 2.93$ nm and the above angles. Two other possible structures encountered in Ni–Mn–Ga alloys, namely 10 M and 2 M [17], do not seem to fit the observed XRD profiles. Moreover, the electron diffraction pattern in figure 3

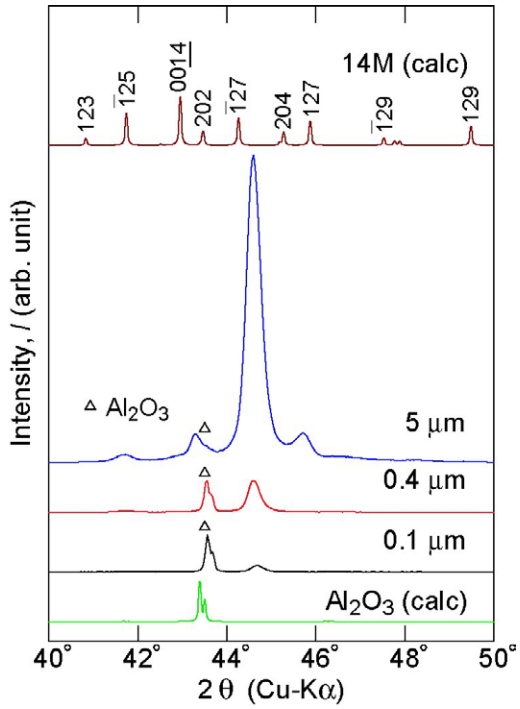

Figure 2. XRD profiles for the annealed $Ni_{53.5}Mn_{23.8}Ga_{22.7}$ films deposited on alumina substrate. The calculated fragments of XRD pattern for 14 M martensite and reflections of Al_2O_3 phase are shown as references.

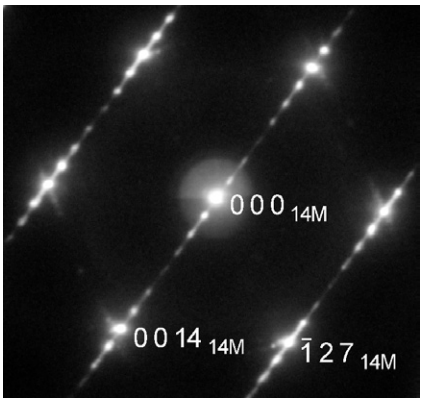

Figure 3. Electron diffraction pattern of the foil prepared from a free-standing 5.0 μm film showing seven-layer modulation of the 14 M martensitic crystal lattice.

clearly shows six extra spots equally spaced, the distance between the fundamental reflections being an unequivocal signature of 14 M martensite. It has to be emphasized that the cluster of peaks shown in figure 2 locates at the 2θ angle position of the former 220 peak of the initial cubic mother phase. This may suggest an inheritance of a crystal texture of austenite by the martensite. The much larger thermal expansion coefficient in Ni–Mn–Ga than in alumina results in an in-plane compression during heating, thus it is natural to assume that the film

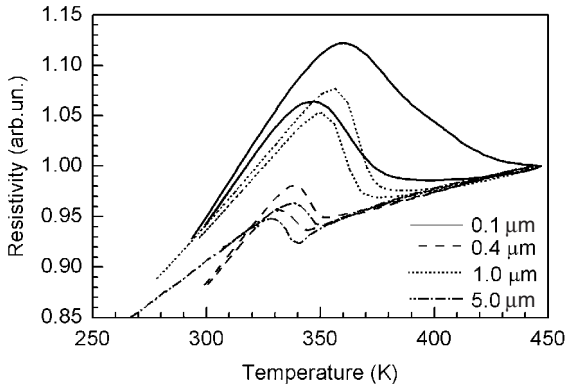

Figure 4. Heating–cooling curves of the normalized electrical resistivity showing a reversible martensitic transformation as a function of film thickness for annealed $Ni_{53.5}Mn_{23.8}Ga_{22.7}$ films deposited on alumina.

Table 1. Transformation and magnetic characteristics of 14 M martensitic $Ni_{53.6}Mn_{23.4}Ga_{23.0}$ thin films attached to an alumina substrate for different film thicknesses. T_{ms} and T_C are the martensitic start and Curie temperature, respectively. M_s is the value of saturation magnetization at 20 kOe and 250 K, A is the magnetic anisotropy of the films calculated from the area between in-plane and out-of-plane $M(H)$ curves, and χ is the initial magnetic susceptibility measured as a slope of the $M(H)$ curves at in-plane low field.

Film thickness, d (μm)	T_{ms} (K)	T_C (K)	M_s (emu cm^{-3})	A ($\times 10^5$, erg cm^{-3})	χ (emu cm^{-3} Oe^{-1})	Domain width, δ (μm)
0.1	377	354	438		0.57	0.21(3)
0.4	343	346	500	6.20	0.34	0.38(6)
1.0	369	360	480	6.62	0.24	0.6(1)
5.0	340	346	522	8.72	0.20	1.5(2)

crystallizes during annealing in such a way that close-packed planes {110} of the initial cubic lattice grow preferably in the plane of the film. This texture for Ni–Mn–Ga films is reported in [6, 18]. Studies are currently under way to confirm the details of texture behaviour of our films.

Temperature dependences of the resistivity show that aforementioned Ni–Mn–Ga martensitic phase is formed in studied films as a result of a martensitic transformation accompanied by anomalies with a narrow temperature hysteresis typical for the bulk alloy (figure 4). The martensitic transformation start temperatures, T_{ms}, determined from figure 4 by the tangential method are listed in table 1. Since the Curie temperatures, T_C, in the studied films are close to the T_{ms} values, the resistivity curves in figure 4 do not show the anomalies produced by ferromagnetic ordering. In order to assess the values of T_C, the temperature dependences of magnetization at the field of 20 kOe depicted in figure 5 were recorded. The values of T_C obtained as the minima of derivatives are listed in table 1. The $M(T)$ dependences may also be used to determine the saturation magnetization. The data taken at 250 K and listed in table 1 are close to the bulk [19].

Figure 6 shows typical examples of magnetic-field-dependent magnetization characteristics. An in-plane magnetic anisotropy was not found in our measurements. The areas between the $M(H)$ curves measured in plane and perpendicular to the film plane are tentatively considered as the magnetic anisotropy energies, A, of the films, which are also summarized in

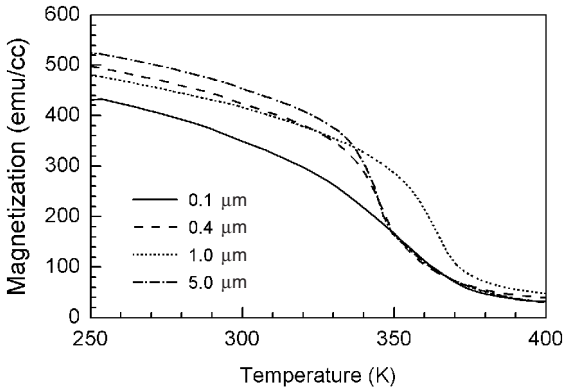

Figure 5. Magnetization versus temperature curves upon heating showing a ferromagnetic transition in annealed $Ni_{53.5}Mn_{23.8}Ga_{22.7}$ films deposited on alumina.

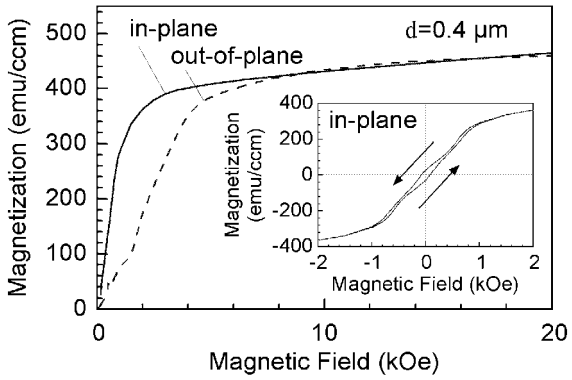

Figure 6. Typical in-plane and out-of-plane $M(H)$ characteristics for the annealed $Ni_{53.5}Mn_{23.8}Ga_{22.7}$ film deposited on alumina. Inset: full hysteresis loop.

table 1. For 0.1 μm, no result is obtained due to experimental limitations of perpendicular measurements. The $M(H)$ behaviour at the low magnetic field range is shown in figure 7 for all films. An initial magnetic susceptibility, χ, was calculated as the slope of the linear parts of the $M(H)$ dependences. Its values are listed in table 1 for each film.

4. Magnetic domain imaging

The magnetic results described in section 3 reflect an averaged behaviour of the thin films. MFM investigations allow a direct access to the some microscopic details of the magnetic structures. Figure 8 shows the magnetic domain structures for all the films under zero applied field. The MFM images reveal a magnetic contrast produced by magnetic stripe domains forming a maze pattern. The magnetic domains represent the regions of uniform magnetization which in our case extend over many grains. Bright and dark regions in the MFM images are associated with the magnetization being parallel or antiparallel to the out-of-plane direction which, in general, can be along the film normal or in the tilted position to it. Comparing the pictures in figure 8, a strong dependence of a stripe period on the film thickness is observed. The averaged widths of magnetic domains measured from the images in figure 8 are shown in

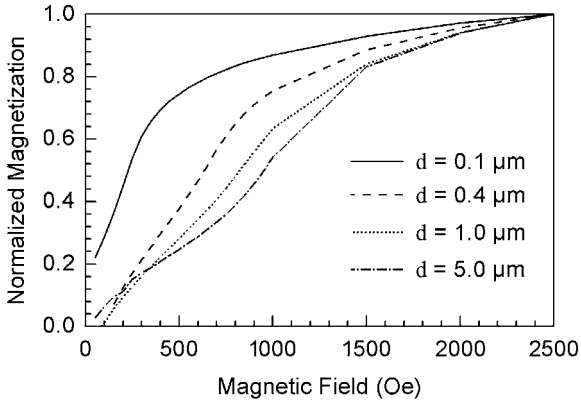

Figure 7. Normalized $M(H)$ dependences taken in the first quadrant of the hysteresis loop for annealed $Ni_{53.5}Mn_{23.8}Ga_{22.7}$ films deposited on alumina.

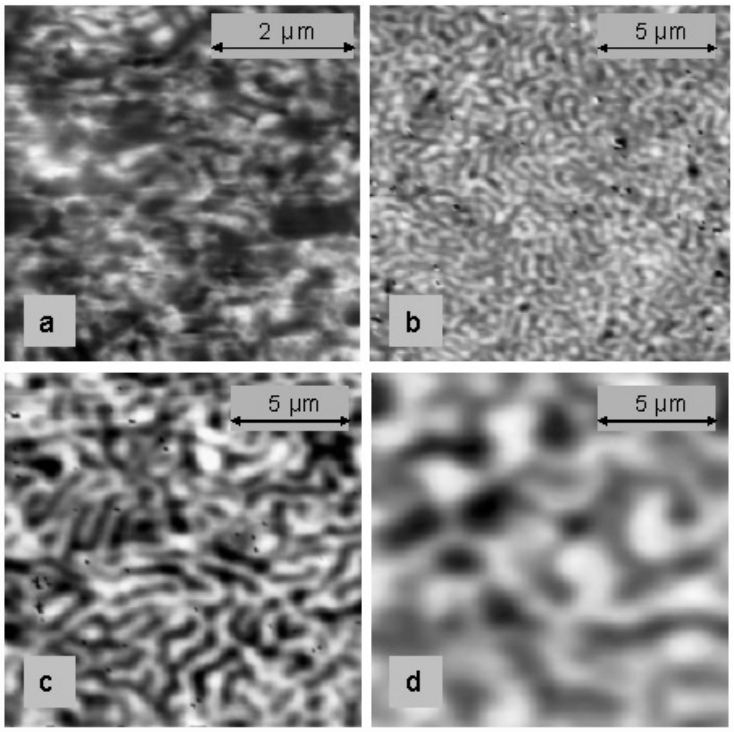

Figure 8. Zero magnetic field MFM images of the domain pattern for annealed $Ni_{53.5}Mn_{23.8}Ga_{22.7}$ martensitic films with different thicknesses: 0.1 μm (a), 0.4 μm (b), 1 μm (c), and 5 μm (d). Note that the frame size is 5×5 μm^2 for case (a) and 15×15 μm^2 for the others.

table 1. As they display a large out-of-plane magnetization component, domains of different polarity must be separated by Bloch domain walls (DWs), which are hardly distinguishable in the images. In contrast to bulk Ni–Mn–Ga alloys [15, 16], no direct morphological relationship between the magnetic domain size or domain configuration and the martensitic microstructure of each grain is observed for the films. Our preliminary results of focused ion beam observations

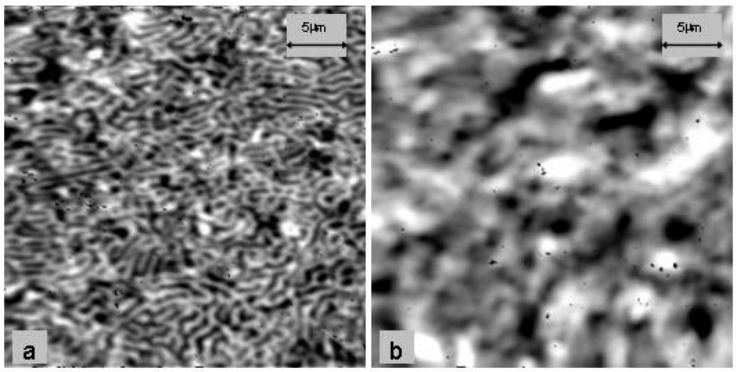

Figure 9. Comparison of the magnetic contrast at zero magnetic field (a) and at a magnetic field of 3.5 kOe applied along the film normal (b) for the film with a thickness of 1 μm.

indicate a perfect in-plane laminated substructure of each grain with the averaged thickness of lamella being about 40 nm, each lamella being a martensitic twin variant. Apparently, this martensitic nanostructure is a result of crystal texture mentioned in section 3. Besides, the crystal texture is the main cause of the uniaxial magnetic anisotropy of the studied films.

The domain features of the films change drastically in the perpendicular magnetic field of a permanent magnet as can be seen from figure 9. The MFM image in figure 9(b) reveals that the magnetization of the film is largely reversed as follows from the ratio of light to dark image contrast.

5. Discussion and conclusions

The main findings of this work are the out-of-plane arrangements of magnetic moments in the Ni–Mn–Ga martensitic films and a thickness dependence of domain width.

An out-of-plane magnetic anisotropy of the films is expected to occur because of the particular film structure and the large magnetic anisotropy of single variants of orthorhombic Ni–Mn–Ga martensite. Incidentally, the demagnetizing factor and substrate influence favour an in-plane alignment of the magnetic moments, especially when causing in-plane compression. As mentioned in section 3, the films represent a fine polycrystalline structure with columnar grains. An analysis of the conditions of recrystallization of the films attached to the substrate and preliminary crystallographic tests suggest an in-plane $\{110\}$ texture in the cubic austenitic phase. Due to the lattice correspondence, the microstructure of martensite bears features of mother phase such as being parallel to the film plane twin boundaries. In this case, the $\langle 100\rangle$-directions must be inclined to the film plane by 45°. The latter fact implies that the shorter axes of the orthorhombic twin variants corresponding to the easy axes for the magnetization will be preferentially aligned in these directions. Thus, the resulting alignment of magnetic moments, domain structure, magnetic properties and their thickness variation in the studied films are dependent on the competitive contribution of magnetic anisotropy energy, exchange energy and dipolar energy effects due to columnar structure, on the one hand, and the magnetostatic energy contributions due to the film shape, on the other. The stripe domain structure with out-of-plane arrangement of the magnetic moments observed in this work represents the simplest strategy of minimization of those energy contributions. In this case, a classical domain theory which considers the domains and domain walls as basic elements with a simple one-dimensional model of a DW is applicable.

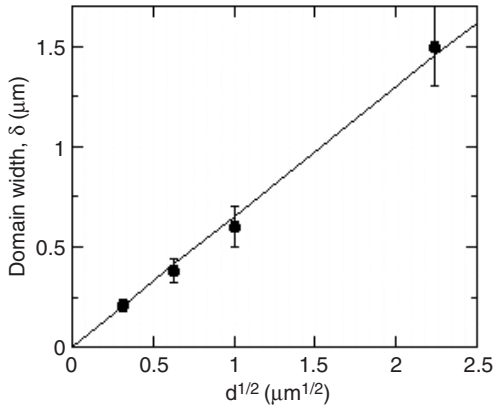

Figure 10. Relationship between the domain width, δ, determined from figure 8, and film thickness, d.

Conventional DW width is mainly determined by the opposite influence of anisotropy and nonuniform exchange energies. In the spirit of references [20, 21], one can deduce the order of magnitude of the DW width, δ_{dw}, from the approximate expression

$$\delta_{dw} \approx a_{av}\sqrt{\frac{E}{A}}, \tag{1}$$

where a_{av} is an average lattice parameter, E is the exchange energy per volume of the unit cell, and A is an overall anisotropy constant. Taking an averaged value of the Curie temperature from table 1, one can roughly evaluate $E \sim 10^{10}$ erg cm^{-3}. With an averaged value of A from table 1 and $a \approx 0.6$ nm as an averaged lattice parameter of Ni–Mn–Ga martensite in the cubic coordinates, equation (1) yields $\delta_{dw} \sim 60$ nm. This value is much smaller than the width of the observed magnetic domains; see table 1. Thus, in a first approximation, the width of the magnetic stripe domains, δ, as a function of the magnetic layer thickness, d, is described by the formula [20, 21]

$$\delta = \xi\sqrt{d}, \tag{2}$$

where ξ is a coefficient relating the parameters characterizing the anisotropy and exchange energies. The numerical value of ξ obtained for the microscopic single-crystalline layer of Fe bounded above and below by $\{111\}$-type planes is equal to 5.5×10^{-3} if d is expressed in the units of centimetres [20].

Figure 10 shows that the experimental results for Ni–Mn–Ga thin films in the submicron range are well described by equation (2). The excellent fit to the predicted behaviour makes one confident in the validity of equation (2) in the whole studied range, although only four samples have been explored by MFM. Extrapolation of the line in figure 10 to zero does not mean *a priori* that equation (2) holds in the whole nanoscale region. It is surprising that in our case ξ is 4.4×10^{-3}, which is fairly close to the aforementioned value. This could mean that, although the magnetic parameters of the cubic single-crystal Fe and orthorhombic polycrystalline Ni–Mn–Ga differ, their combined influences on the domain structure in thin layers are similar.

The data of table 1 evidence the trend in the thickness dependence of overall anisotropy energy, A, and initial magnetic susceptibility, χ. For thickness of 0.4 mm, the anisotropy energy reduces by about 30%. This trend is correlated with the averaging of the local anisotropies. Nevertheless, the occurrence of stripe domains with a width larger than the film thickness

in the case of a 0.1 μm thick film still suggests a high enough anisotropy for an out-of-plane alignment of magnetic moments in this thinnest film studied in the present work. It is noteworthy that, comparative to the other films, the roughness of the substrate in the latter case may contribute more to disturbance of the parallel alignment of twin boundaries with regard to the film plane, and that the stripe domain structure appears less developed (see figure 8). The observed increase of the in-plane and out-of-plane low-field magnetic susceptibilities for thinner films is in line with these conclusions.

In summary, submicron films of ferromagnetic Ni–Mn–Ga martensites attached to alumina substrates have been prepared. As in a bulk state of a similar composition, they exhibit a 14 M martensitic phase formed as a result of the reversible MT with a small temperature hysteresis and narrow temperature intervals of the forward and reverse transformations. The thin film state of martensitic films and their firm connection to the alumina substrate cause so-called submicron anomalies found in this and our recent work: the submicron thickness dependences of the transformation temperatures, critical fields, susceptibilities and anisotropies [7, 8]. Structurally, Ni–Mn–Ga thin films are characterized by the higher preference of in-plane 110-texture.

The MFM observations reveal a stripe domain structure with the domain width changing as a square root function of the film thickness. Currently, magnetomechanical tests are under way to clarify the potential of these films for applications.

Acknowledgment

The authors are grateful to G Kourliandskaia for help in the processing of MFM images.

References

[1] Isokawa S, Suzuki M, Ohtsuka M, Matsumoto M and Itagaki K 2001 *Mater. Trans.* **42** 1886
[2] Ohtsuka M, Sanada M, Matsumoto M and Itakagi K 2004 *Mater. Sci. Eng.* A **378** 377
[3] Rumpf H, Feydt J, Levandovski D, Ludwig A, Winzek B, Quandt E, Zhao P and Wuttig M 2003 Smart structures and materials: active materials: behavior and mechanics *Proc. SPIE* vol 5053, ed D C Lagoudas (Bellingham, WA: SPIE Optical Engineering Press) p 191
[4] Tello P, Castano F J, O'Handley R C, Allen S M, Esteve M, Castano F, Labarta A and Battle X J 2002 *Appl. Phys.* **91** 8234
[5] Wuttig M, Craciunescu C and Li J 2000 *Mater. Trans. JIM* **41** 933
[6] Dubowik J, Kudryavtsev Y V and Lee Y P 2004 *J. Appl. Phys.* **95** 2912
[7] Chernenko V A, Ohtsuka M, Kohl M, Khovailo V V and Takagi T 2005 *Smart Mater. Struct.* at press
[8] Kohl M, Chernenko V A, Ohtsuka M, Reuter H and Takagi T 2005 *Mater. Res. Soc. Symp. Proc.* **855E** W2.8.1
[9] Kohl M, Hoffmann S, Liu Y, Ohtsuka M and Takagi T 2003 *J. Physique Coll.* IV **112** 1185
[10] Kohl M, Liu Y, Krevet B, Dürr S and Ohtsuka M 2004 *J. Physique Coll.* IV **115** 333
[11] Ullakko K, Huang J K, Kantner C, O'Handley R C and Kokorin V V 1996 *Appl. Phys. Lett.* **69** 1966
[12] Müllner P, Chernenko V A and Kostorz G 2004 *J. Appl. Phys.* **95** 1531
[13] Pan Q and James R D 2000 *J. Appl. Phys.* **87** 4702
[14] Park H S, Murakami Y, Shindo D, Chernenko V A and Kanomata T 2003 *Appl. Phys. Lett.* **83** 3752
[15] Ge Y, Heczko O, Soderberg O and Lindroos V K 2004 *J. Appl. Phys.* **96** 2159
[16] Sullivan M R, Ateya D A, Pirota S J, Shah A A, Wu G H and Chopra H D 2004 *J. Appl. Phys.* **95** 6951
[17] Pons J, Chernenko V A, Santamarta R and Cesari E 2000 *Acta Mater.* **48** 3027
[18] Ahn J-P, Cheng N, Lograsso T and Krishnan K M 2001 *IEEE Trans. Magn.* **37** 2141
[19] Chernenko V A, L'vov V A, Zagorodnyuk S P and Takagi T 2003 *Phys. Rev.* B **67** 064407
[20] Lifshitz E 1944 *J. Physique* **8** (6) 337
[21] Solzi M, Ghidini M and Asti G 2002 Macroscopic magnetic properties of nanostructures and nanocomposite systems *Magnetic Nanostructures* ed H S Nalwa (Stevenson Ranch, CA: ASP)